Phase-controlled Epitaxial Lateral Overgrowth of α-Ga_2O_3 by Halide Vapor Phase Epitaxy

Yuichi Oshima,[1*] Katsuaki Kawara,[2] Takayoshi Oshima,[2] Mitsuru Okigawa,[2] Takashi Shinohe[2]

[1]*Optical Single Crystals Group, National Institute for Materials Science, 1-1 Namiki, 305-0044 Tsukuba, Japan*

[2]*FLOSFIA, Inc., 1-29 Goryoohara, Nishikyo-ku, 615-8245 Kyoto, Japan*

E-mail: OSHIMA.Yuichi@nims.go.jp

We investigated the effect of mask materials on the epitaxial lateral overgrowth (ELO) characteristics of α-Ga_2O_3 and developed an ELO technique that can markedly suppress abnormal growth and cracking to enable long-term growth on a wide mask, which is necessary to effectively improve the crystal quality. A conventional SiO_x mask provided excellent growth selectivity with only a thin amorphous GaO_x layer on the mask between α-Ga_2O_3 islands. However, the amorphous layer transformed into β-Ga_2O_3, which disrupted the long-term growth of α-Ga_2O_3. Amorphous deposition was avoided by using a TiO_x mask. When a TiO_x mask was used, κ-Ga_2O_3 deposited on the mask, and no transformation to β-Ga_2O_3 was observed. α-Ga_2O_3 islands with a diameter as large as approximately 25 μm were grown by the developed ELO technique using a TiO_x mask. Transmission electron microscopy observation did not detect dislocations in the outermost part of the islands.

1. Introduction

Corundum-structured α-Ga_2O_3 is an ultra-wide bandgap semiconductor with a bandgap energy E_g of 5.3 eV.[1)] α-Ga_2O_3 is expected to possess a very high breakdown field because of its large E_g, and therefore α-Ga_2O_3 is promising for high-performance power device applications. Indeed, α-Ga_2O_3-based Schottky barrier diodes with very low on-resistance have already been demonstrated.[2)] Because corundum is a common crystal structure, there are many other corundum-structured oxides with which α-Ga_2O_3 can form solid solutions. For example, α-$(Al_xGa_{1-x})_2O_3$ can be grown without any limitation of the Al content,[3, 4)] in contrast to the case of β-$(Al_xGa_{1-x})_2O_3$.[5-7)] Although it would be impossible for α-Ga_2O_3 to display *p*-type conduction, as is the case for β-Ga_2O_3, corundum-structured *p*-type oxides, such as α-Ir_2O_3 or α-Rh_2O_3 are available to make *pn* heterojunctions.[8-10)] For example, normally-off metal-oxide-semiconductor field-effect transistors with a *p*-type well layer have been demonstrated.[11, 12)]

To use α-Ga_2O_3 for device applications, it is essential to establish an epitaxial growth technique that can grow high-quality α-Ga_2O_3 epilayers with controlled conductivity at a reasonably high growth rate. To date, epitaxial growth of α-Ga_2O_3 has mainly been performed by mist chemical vapor deposition (CVD)[1, 4, 10)] or halide vapor phase epitaxy (HVPE).[13-15)] α-Ga_2O_3 needs to be grown heteroepitaxially, typically on sapphire substrates, because α-Ga_2O_3 is metastable at ambient pressure[16, 17)] and melt-grown native substrates are not available, in contrast to the case of β-Ga_2O_3. The dislocation density in such a heteroepitaxial α-Ga_2O_3 layer is typically as high as 10^{10} cm^{-2} if no measure is taken because of the large lattice mismatch ($\Delta a/a$ ~4.5%, $\Delta c/c$ ~3.3%).[18)] Accordingly, the crystal quality needs to be improved to fully exploit the potential of α-Ga_2O_3. To decrease the dislocation density, an epitaxial lateral overgrowth (ELO) technique for α-Ga_2O_3 has been investigated .[18-21)] Using ELO, the dislocation density of α-Ga_2O_3 was decreased to below 5×10^6 cm^{-2} in the laterally grown wing regions.[18)] However, the ELO technique is still its infancy. For example, the dislocation density was still high in the window regions even after facet-initiated ELO[22)] was used to bend the dislocations that propagated into α-Ga_2O_3 islands through the windows,[18)] which limited the high-quality area.

An effective way to lower the fraction of the low-quality area of α-Ga_2O_3 is to use a mask with a smaller fill factor (i.e., a wider mask with smaller/fewer windows) in the ELO process. The resulting decrease of island density will also help to lower the tensile strain, which is caused by the surface tension generated upon island coalescence[23)] and can induce bowing

and/or cracking of the α-Ga_2O_3 epilayer. To achieve island coalescence and obtain a compact layer on a mask with a small fill factor, a long growth period is required. However, as described later, such long-term growth is disrupted by abnormal growth when a conventional SiO_x mask is used.

In the present work, we investigate the origin of the abnormal growth on the SiO_x mask during the ELO process of α-Ga_2O_3. We clarify that the abnormal growth is caused by the crystallization of deposited amorphous GaO_x into β-Ga_2O_3 on the mask. To solve this problem, we develop an ELO technique in which polycrystalline κ-Ga_2O_3 (orthorhombic ε-Ga_2O_3) is intentionally deposited on a TiO_x mask between α-Ga_2O_3 islands.

2. Experimental methods

We used HVPE to grow Ga_2O_3 in the present work. HVPE is a type of CVD that is characterized by a rapid growth rate. HVPE has been widely used to grow thick layers of III-V semiconductors such as GaN and AlN.[24-26] In 2015, Oshima et al. reported the first example of HVPE of α-Ga_2O_3 and demonstrated a very high growth rate of over 100 μm/h .[13]

ELO of α-Ga_2O_3 was performed in an atmospheric horizontal quartz HVPE reactor at 520–540 °C. O_2 (>99.9999% pure) and GaCl were supplied as precursors together with N_2 as the carrier gas. GaCl was synthesized upstream in the reactor through the chemical reaction between metal Ga (>99.99999% pure) and HCl gas (>99.999% pure) at 570 °C. Additional HCl was supplied together with the precursors to suppress gas-phase parasitic reactions.[27] The partial pressures of GaCl, O_2, and additional HCl were 1.25×10^{-1}, 1.25, and 1.25×10^{-1} kPa, respectively, unless otherwise specified. The growth rate of a flat α-Ga_2O_3 film under the growth conditions described above was 12 μm/h.

First, a 3-μm-thick α-Ga_2O_3 seed layer was grown by HVPE on a patterned sapphire substrate (PSS). We used a PSS to prevent the grown film from peeling off the substrate because of intrinsic and/or thermal stress. Second, an SiO_x or TiO_x mask pattern was formed on the seed layer using conventional photolithography. The SiO_x film (10-nm thick) or TiO_x film (10- or 50-nm thick) was deposited by sputtering. Figure 1 shows the mask pattern. The triangular-lattice mask pattern was aligned such that a side of a triangle was parallel to the $<11\bar{2}0>$ direction of α-Ga_2O_3. The circle window diameter was fixed at 5 μm. The mask width (the distance between mask edges of the nearest windows) was 5–20 μm. Finally, a second HVPE step was performed on the α-Ga_2O_3 template with the mask.

Sample morphology was observed by scanning electron microscopy (SEM). The crystal structure of the grown crystals and their orientation was investigated by electron backscatter diffraction (EBSD) and selected-area electron diffraction (SAED) analyses combined with transmission electron microscopy (TEM).

3. Results and discussion

3.1 Growth with an SiO_x mask

Figure 2(a)–(c) show SEM images of α-Ga_2O_3 islands grown for 20 min at 540 °C on an α-Ga_2O_3 template with an SiO_x mask (width of 10 μm). The growth selectivity appeared to be high in Fig. 2(a); however, Fig. 2(b) and (c) revealed the existence of a thin layer deposited on the mask. As explained later, the deposited layer was amorphous GaO_x. This amorphous layer became thicker with decreasing growth temperature, which is probably because of the decrease of thermal desorption of surface atoms from the amorphous layer and/or increase of precursor delivery caused by the growth rate decrease of the α-Ga_2O_3 islands at low temperatures.[13] The amorphous layer also became thicker as the mask width increased, which was probably caused by the increase of precursor delivery on the mask because the precursor consumed in growth of α-Ga_2O_3 islands decreased. The amorphous layer thickness tended to saturate with lengthening growth time, which was most likely because the precursor supply to the mask was shaded when the α-Ga_2O_3 islands got thicker. It is noteworthy that the amorphous layer was not observed under the α-Ga_2O_3 islands, as shown in Fig. 2(b) and (c). There was a void between the amorphous layer and periphery of the α-Ga_2O_3 island bottom. The amorphous layer had a steep edge that faced the void. Similar void structure was always observed at the periphery of the island bottom when the growth time was extended. This indicates that the void moved laterally with the increase of island diameter. Accordingly, the area of the amorphous layer became smaller.

Figure 3 depicts a schematic of the growth model elucidated from the observations described above. At the beginning of island growth, a large proportion of the precursors should be consumed to grow α-Ga_2O_3 islands near the mask edge. As a result, the amorphous layer gradually became thinner near the mask edge (Fig. 3(a)). Therefore, the amorphous layer should not have a steep edge at this stage. Once the mask edge is covered by the α-Ga_2O_3 island periphery (Fig. 3(b)), precursor supply to the amorphous layer edge is suppressed, and a steep edge will be formed by the thermal evaporation of the surface atoms (Fig. 3(c)). At the same time, α-Ga_2O_3 homoepitaxially grows on the α-Ga_2O_3 face in the void using the

Ga and O atoms supplied from the amorphous layer edge. As a result, the void moves laterally and stays at the periphery of the α-Ga_2O_3 islands during their lateral growth (Fig. 3(d)).

Figure 4(a) presents a cross-sectional TEM image of the deposited layer on the SiO_x mask. The deposited layer on the mask showed virtually no contrast, whereas a high density of dislocations was observed in the α-Ga_2O_3 seed layer. A SAED pattern of the deposited layer on the mask exhibited a halo pattern (Fig. 4(b)), indicating that the layer was amorphous. The α-Ga_2O_3 seed layer showed the well-ordered spotted SAED pattern expected for single-crystalline α-Ga_2O_3.

Unfortunately, long-term growth of α-Ga_2O_3 islands using an SiO_x mask was disrupted by abnormal growth. Figure 5(a) presents an SEM image that shows the beginning of the abnormal growth. The sample was grown using the same growth recipe with that for the sample shown in Fig. 2, except that a wider SiO_x mask (20-μm-wide) was used. A part of the deposited layer on the mask exhibited brighter contrast than that of the surrounding amorphous layer and cracking along non-random directions was observed, indicating the crystallization of the amorphous layer. Such crystallization was found much more frequently compared to the case of the sample shown in Fig. 2. This is probably because of the volume increase of the amorphous layer associated with the use of the wider mask. Figure 5(b) displays an SEM image of part of the same sample with a well-formed crystallized deposited layer. The deposited layer clearly exhibited facets. Further growth of this deposited layer led to the abnormal growth of α-Ga_2O_3 islands (circled area in Fig. 5(c), grown for 2h using a 10-μm-wide mask). The abnormal growth tended to increase with increasing the growth temperature, growth duration, and mask width. The abnormal growth finally dominated the overall growth, and the ELO process was disrupted.

Figure 6(a) and (b) show cross-sectional SEM images of part of the sample where the abnormal growth just started (the same sample as is shown in Fig. 5(a) and (b)). Figure 6(b) is a magnified image of the area where the deposited layer on the mask crystallized. The deposited layer partially peeled off, and the seed layer had some cracks. Figure 6(c) presents a material map of the area shown in Fig. 6(b) obtained by EBSD measurements. The map revealed that the amorphous layer on the mask turned into β-Ga_2O_3. Because amorphous GaO_x should be less stable than crystalline Ga_2O_3, it is reasonable that the amorphous layer turns into crystalline Ga_2O_3, although the trigger for this transformation is unknown at present. Because the crystal structure of Ga_2O_3 should not be restricted upon crystallization on the amorphous SiO_x mask, it is reasonable that the resulting polymorph is the most stable

β-phase. β-Ga_2O_3 was also found in the seed layer. The cracking in the seed layer is probably because of the stress caused by the volume increase associated by the phase transition from α-Ga_2O_3 to β-Ga_2O_3, the theoretical specific volume of which are 0.155 and 0.170 cm^3/g, respectively. At present, it is not clear where the phase transition was initiated.

3.2 ELO of α-Ga_2O_3 with an epitaxial κ-Ga_2O_3 layer on a thin TiO_x mask

To effectively decrease the dislocation density by ELO, the mask fill factor should be small. However, in the case of the SiO_x mask, the risk of abnormal growth increased as the fill factor decreased because the area of the amorphous layer increased. Accordingly, the deposition of the amorphous layer needs to be avoided. We found that crystalline Ga_2O_3 grew epitaxially on the mask when a thin (~10 nm) TiO_x layer was used instead of SiO_x. As explained later, the crystalline Ga_2O_3 was the κ-phase (orthorhombic ε-Ga_2O_3). Figure 7(a)–(f) present the time evolution of the ELO process up to 40 min using a thin TiO_x mask (width of 10 μm) at 540 °C. Growth of a flat layer with some misoriented 3D grains was observed on the mask between α-Ga_2O_3 islands. When compared at the same growth time, the deposition thickness (Fig. 7(d)) was much thicker than that of the amorphous layer on the SiO_x mask shown in Fig. 2. The growth rate of α-Ga_2O_3 islands was faster than that of the deposited layer on the mask, and therefore the ELO process was successful.

Figure 8(a) presents a cross-sectional TEM image of the sample shown in Fig. 7(c) and (d). The TEM specimen was prepared so that the flat layer deposited on the mask and a 3D grain were observed at the same time. Note that no α-Ga_2O_3 islands were included. A high density of dislocations was observed in the layer deposited on the mask and α-Ga_2O_3 seed layer, whereas their density was much lower in the 3D grain. Figure 8(b) depicts a SAED pattern of the flat layer deposited on the mask. The pattern agreed with that of κ-Ga_2O_3 with <110> incidence. The lateral streak indicates a domain structure with small lateral size. The orientation relationships between the flat κ-Ga_2O_3 and α-Ga_2O_3 seed layers were κ(001) || α(0001) and κ<110> || α<11$\bar{2}$0>. Figure 8(c) presents a SAED pattern of the 3D grain. This pattern agreed with that of κ-Ga_2O_3 with <113> incidence. Figure 8(d) and (e) present SAED patterns of the seed layer and substrate, respectively. These patterns were consistent with corundum structure with <11$\bar{2}$0> incidence.

It is known that TiO_x crystallizes at much lower temperatures than SiO_x.[28, 29] In addition, it is likely that the thin TiO_x layer was deposited on the seed layer almost epitaxially because of its small thickness, leading to the well-oriented deposition of κ-Ga_2O_3. κ-Ga_2O_3 should

be more stable than amorphous GaO_x and no transition from κ-Ga_2O_3 to β-Ga_2O_3 was observed, unlike for the case of the SiO_x mask. However, the samples suffered from serious cracking during growth even before island coalescence and long-term growth was more difficult than when an SiO_x mask was used. In the case of heteroepitaxial GaN, the GaN layer is subjected to large tensile strain because of the decrease of the edge dislocation density along the growth direction.[30] In the present case, the dislocation density of the κ-Ga_2O_3 layer was very high, as shown in Fig. 8(a), and therefore tensile strain can be induced by a similar mechanism. In the case of conventional ELO, although tensile strain can be generated at each α-Ga_2O_3 island, the strain can be locally relieved by the shrinkage of each island, and therefore the tensile strain would not be large until island coalescence. However, in the present case, α-Ga_2O_3 islands and the κ-Ga_2O_3 layer are connected to each other even before island coalescence and the κ-Ga_2O_3 layer also increases the tensile strain. Therefore, the tensile strain should be much greater than that in a sample grown by conventional ELO, leading to the serious cracking.

3.3 ELO of α-Ga_2O_3 with a polycrystalline κ-Ga_2O_3 layer on a thick TiO_x mask

To suppress the tensile strain in the samples, it would be effective to deposit polycrystalline κ-Ga_2O_3 on the mask instead of epitaxial κ-Ga_2O_3 because the dislocation density in a 3D κ-Ga_2O_3 grain is much lower than that in an epitaxial κ-Ga_2O_3 layer, as shown in Fig. 8(a), which means that the tensile strain generated by the decrease in edge dislocation density should be much smaller. Accordingly, we examined the use of a 50-nm-thick TiO_x mask, the crystal orientation of which should be much more disordered than that of the 10-nm-thick TiO_x layer. Figure 9(a) and (b) present SEM images of a sample grown for 40 min at 540 °C using a 50-nm-thick TiO_x mask with a width of 20 μm. Polycrystalline κ-Ga_2O_3 grew on the mask between α-Ga_2O_3 islands. The κ-Ga_2O_3 should be buried by growth for a sufficiently long time because the growth rate of the α-Ga_2O_3 islands was higher than that of the κ-Ga_2O_3 layer, as shown in Fig. 9(b), although the lateral growth rate of α-Ga_2O_3 islands was lower than those in the two cases described in Section 3.1 and 3.2.

The SEM images in Fig. 10(a)–(f) illustrate the time evolution of the growth up to 5h at 520 °C using a 50-nm-thick TiO_x mask (width of 20-μm). Note that not only α-Ga_2O_3 islands but κ-Ga_2O_3 grains also grew larger with increasing the growth duration. It was possible to grow the sample for over 5 h without any abnormal growth or cracking. As a result, α-Ga_2O_3 islands with a diameter as large as approximately 25 μm were grown and they coalesced

with each other. In contrast, it was difficult to grow samples for over 40 min when a 10-nm-thick TiO_x mask was used.

Figure 11(a) presents an SEM image of a sample grown using an SiO_x mask (10-μm-width) for 1 h at 540 °C. Abnormally grown α-Ga_2O_3 islands were easily found. Regions where the abnormal growth was significant were observed as white spots to the naked eye (Fig. 11(b)). Conversely, no abnormal growth was found when the 50-nm thick TiO_x mask (10-μm-width) was used under the same growth conditions (Fig. 11(c) and (d)). Thus, this ELO technique in which polycrystalline κ-Ga_2O_3 is intentionally deposited on the mask effectively suppresses both the abnormal growth and cracking to enable a long growth period. As a result, large lateral-sized islands were obtained when a mask with a small fill factor was used and the dislocation density should be decreased effectively.

Figure 12(a) presents a cross-sectional TEM image of a region containing the edges of α-Ga_2O_3 islands that were about to coalesce with each other. Figure 12(b) shows the part of the sample from which the TEM specimen was cut. The mask width was 20 μm, which was much wider than the previously reported mask (5 μm).[18] No dislocations were detected in the α-Ga_2O_3 areas, including the α-Ga_2O_3/κ-Ga_2O_3 boundaries, indicating that a wide high-quality area was achieved. Although we have not performed TEM observation in the central part of an α-Ga_2O_3 island, the behavior of dislocations propagated through a mask window should be similar to that in the case of a conventional SiO_2 mask.[18] Note that the κ-Ga_2O_3 grains between the α-Ga_2O_3 islands also grew so large that only a few grains were observed in the TEM image. No defect contrasts were observed in each single crystalline κ-Ga_2O_3 grain probably because the grain was formed by spontaneous nucleation.

In the ELO process developed here, the lateral growth rate of α-Ga_2O_3 islands is slower than that in conventional ELO and it takes a longer time to achieve island coalescence. Therefore, this technique should be combined with rapid growth. Figure 13(a) and (b) present SEM images of samples grown at a high growth rate of 75 μm/h. SEM images of samples grown at a conventional growth rate of 12 μm/h are also shown for comparison (Fig. 13(c) and (d)). The growth time was adjusted so that the nominal thickness of each sample was similar. No marked differences between the samples were found, except that the sample grown at the higher growth rate possessed smoother facets than that grown at the lower growth rate. Thus, the developed ELO technique can be performed at high growth rate and still achieve effective island coalescence.

4. Conclusions

We investigated the effect of the mask material on the ELO characteristics of α-Ga_2O_3 fabricated by HVPE. A conventional SiO_x mask facilitated excellent growth selectivity; however, the thin amorphous layer deposited on the mask turned into β-Ga_2O_3 and caused abnormal growth, which affected the long-term growth of α-Ga_2O_3. The use of a thin TiO_x mask suppressed the deposition of the amorphous layer and the abnormal growth by covering the mask with an epitaxial κ-Ga_2O_3 layer. However, the resulting samples suffered from serious cracking even before island coalescence, probably because of the tensile strain caused by the decrease of edge dislocation density for both the α-Ga_2O_3 islands and κ-Ga_2O_3 layer. As a result, the maximum growth time was limited, and was even shorter than when an SiO_x mask was used. The cracking was effectively suppressed by depositing polycrystalline κ-Ga_2O_3 on a thick TiO_x mask instead of an epitaxial κ-Ga_2O_3 layer. The growth rate of α-Ga_2O_3 islands was faster than that of the polycrystalline κ-Ga_2O_3 layer, so the κ-Ga_2O_3 layer was buried upon island coalescence. The possible growth period was markedly elongated using this ELO technique and α-Ga_2O_3 islands with a diameter as large as approximately 25 μm were grown. No dislocations were observed in the outermost part of the islands. Increasing the growth rate from 12 to 75 μm/h did not affect the ELO process. This ELO technique in which a polycrystalline κ-Ga_2O_3 layer is intentionally deposited on the mask to suppress abnormal growth and cracking enables a long growth period. Thus, this technique is promising to effectively decrease dislocation density using a mask with a small fill factor.

Acknowledgments

Part of this work is based on results obtained from a project commissioned by the New Energy and Industrial Technology Development Organization (NEDO). Part of this work was supported by the Innovative Science and Technology Initiative for Security, ATLA, Japan. This work was also partly supported by Grants-in-Aid for Scientific Research (C) (No. 17K05047) from the Japan Society for the Promotion of Science (JSPS).

References

1) D. Shinohara and S. Fujita, Jpn. J. Appl. Phys. **47**, 7311 (2008).
2) M. Oda, R. Tokuda, H. Kambara, T. Tanikawa, T. Sasaki, and T. Hitora: Appl. Phys. Express **9**, 021101 (2016).
3) H. Ito, K. Kaneko, S. Fujita, Jpn. J. Appl. Phys. **51**, 100207 (2012).
4) S. Fujita and K. Kaneko, J. Cryst. Growth **401**, 588 (2014).
5) V. G. Hill, R. Roy, and E. F. Osborn, J. Am. Ceram. Soc. **35**, 135 (1952).
6) S. W. Kaun, F. Wu, and J. S. Speck, J. Vac. Sci. Technol. A33, 041508 (2015).
7) R. Miller, F. Alema, and A. Osinsky, IEEE Trans. Semicond. Manufacturing, **31**, 467 (2018).
8) F. P. Koffyberg, Phys. Chem. Solids **53**, 1285 (1992).
9) R. K. Kawar, P. S. Chigare, and P. S. Patil, Appl. Surf. Sci. **206**, 90 (2003).
10) K. Kaneko, S. Fujita, and T. Hitora, Jpn. J. Appl. Phys. **57**, 02CB18 (2018).
11) FLOSFIA and Kyoto univ: News release, July 13 (2008). http://flosfia.com/20180713/
12) FLOSFIA: News release, December 12 (2019). http://flosfia.com/20191202-2/
13) Y. Oshima, E. G. Villora, and K. Shimamura, Appl. Phys. Express **8**, 055501 (2015).
14) A. I. Pechnikov, S. I. Stepanov, A. V. Chikiryaka, M. P. Scheglov, M. A. Odnobludov, and V. I. Nikolaev, Semiconductors **53**, 780 (2019).
15) H. Son and D. W. Jeon, J. Alloys Compd. **773**, 631 (2019)
16) R. Roy, V. G. Hill, and E. F. Osborn, J. Am. Chem. Soc. **74**, 719 (1952).
17) D. Machon, P. F. McMillan, B. Xu, and J. Dong, Phys. Rev. B **73**, 094125, (2006).
18) Y. Oshima, K. Kawara, T. Shinohe, T. Hitora, M. Kasu, S. Fujita, APL mater. **7**, 022503 (2019).
19) H. Son, Y. J. Choi, J. S. Ha, S. H. Jung, and D. W. Jeon, Cryst. Growth Des. **19**, 5105 (2019).
20) A. N. Cha, S. Bang, H. Rho, H. Bae, D. W. Jeon, J. W. Ju, S. K. Hong, and J. S. Ha, Appl. Phys. Lett. **115**, 091605 (2019).
21) R. Jinno, N. Yoshimura, K. Kaneko and S. Fujita, Jpn. J. Appl. Phys. 58, 120912 (2019).
22) A. Usui, H. Sunakawa, A. Sakai, and A. A. Yamaguchi, Jpn. J. Appl. Phys. **36**, L899 (1997).
23) T. Böttcher, S. Einfeldt, S. Figge, R. Chierchia, H. Heinke and D. Hommel, Appl. Phys. Lett. **78**, 1976 (2001).
24) Y. Oshima, T. Eri, M. Shibata, H. Sunakawa, K. Kobayashi, T. Ichihashi, A. Usui, Jpn. J. Appl. Phys **42**, L1 (2003).

25) T. Yoshida, Y. Oshima, K. Watanabe, T. Tsuchiya, and T. Mishima, phys. stat. sol. C **8**, 2110 (2011).
26) Y. Kumagai, Y. Kubota, T. Nagashima, T. Kinoshita, R. Dalmau, R. Schlesser, B. Moody, J. Xie, H. Murakami, A. Koukitu, and Z. Sitar, Appl. Phys. Express **5**, 055504 (2012).
27) Y. Oshima, K. Kawara, T. Oshima, M. Okigawa, T. Shinohe, submitted for publication.
28) M. Higuchi and Y. Azuma, J. Cerm. Soc. Jpn, **105**, 385 (1997).
29) H. Zhang and J. F. Banfield, Chem. Mater. **14**, 4145 (2002).
30) S. Hearne, E. Chason, J. Han, J. A. Floro, J. Figiel. J. Hunter, H. Amano and I. S. T. Song, Appl. Phys. Lett. **74**, 356 (1999).

Figure Captions

Fig. 1. Mask pattern used for α-Ga_2O_3 island growth.

Fig. 2. (a) SEM images of α-Ga_2O_3 islands grown for 20 min at 540 °C using an SiO_x mask (width of 10 μm). (b) Cross-sectional SEM image of an island and (c) a magnified image of the edge of the island bottom.

Fig. 3. Schematic of the proposed mechanism of void formation and lateral void movement.

Fig. 4. (a) Cross-sectional TEM image of an α-Ga_2O_3 template with an SiO_x mask after HVPE growth. SAED patterns of (b) the deposited layer on the mask and (c) the α-Ga_2O_3 seed layer.

Fig. 5. SEM images of α-Ga_2O_3 islands with abnormal growth prepared at 540 °C using an SiO_x mask. Samples grown for (a), (b) 20 min using a 20-μm-wide mask and (c) 2 h using a 10-μm-wide mask.

Fig. 6. (a) SEM image of an α-Ga_2O_3 island grown using an SiO_x mask. (b) Magnified image of the seed layer. (c) Material map obtained by EBSD analysis.

Fig. 7. SEM images of α-Ga_2O_3 islands grown at 540 °C for (a) 5 min, (b) 20 min, and (c) 40 min using a 10-nm-thick TiO_x mask (width of 10 μm).

Fig. 8. (a) Cross-sectional TEM image of an α-Ga_2O_3 template with a 10-nm-thick TiO_x mask after HVPE growth. SAED patterns of the (b) flat deposition layer on the mask, (c) 3D crystal grain, (d) α-Ga_2O_3 seed layer, and (e) sapphire substrate.

Fig. 9. SEM images of α-Ga_2O_3 islands grown for 40 min at 540 °C using a 50-nm-thick TiO_x mask (width of 20 μm).

Fig. 10. SEM images of α-Ga_2O_3 islands grown at 520 °C for (a), (b) 40 min, (c), (d) 2 h, and (e), (f) 5 h using a 50-nm-thick TiO_x mask (width of 20-μm).

Fig. 11. SEM images and appearance of samples grown at 540 °C using (a), (b) an SiO_x mask and (c), (d) a 50-nm-thick TiO_x mask under the same growth conditions. The mask width was 10 μm. Abnormally grown islands are indicated by dotted circles.

Fig. 12. (a) Cross-sectional TEM image of α-Ga_2O_3 islands with κ-Ga_2O_3 grains between them. The sample was grown at 540 °C for 5 h using a 50-nm-thick TiO_x mask (width of 20 μm). Note that the TEM specimen was prepared using the same epi-wafer shown in Fig. 10(e) and (f), but the islands were still separated from each other because this part was not cut from the center of the islands. (b) Schematic showing where the specimen was cut from the epi-wafer.

Fig. 13. SEM images of α-Ga_2O_3 islands grown using a 50-nm-thick TiO_x mask at growth rates of (a), (b) 75 μm/h for 48 min and (c), (d) 12 μm/h for 5 h. Note that (d) is the same image as Figure 9(e).

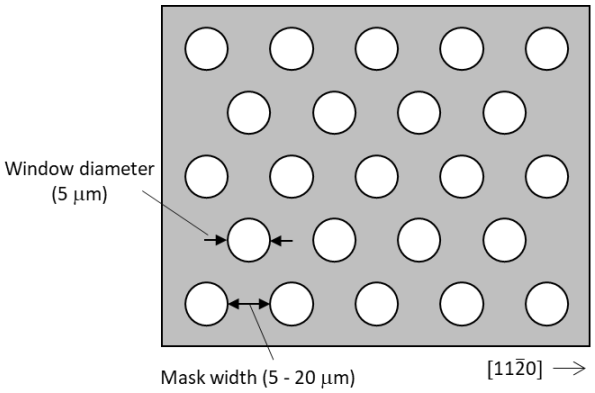
Window diameter
(5 μm)
Mask width (5 - 20 μm)
[11$\bar{2}$0]

Fig. 1.

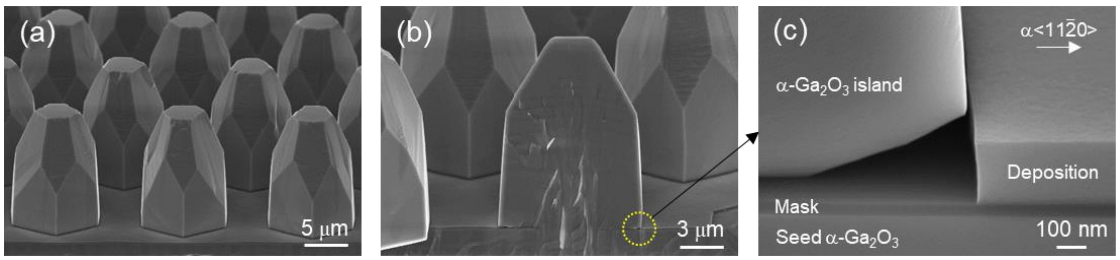
(a)
5 μm
(b)
3 μm
(c)
α<11$\bar{2}$0>
α-Ga_2O_3 island
Deposition
Mask
Seed α-Ga_2O_3
100 nm

Fig. 2.

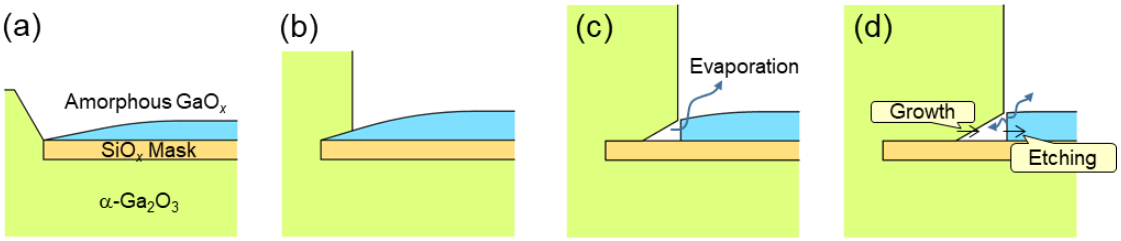

Fig. 3.

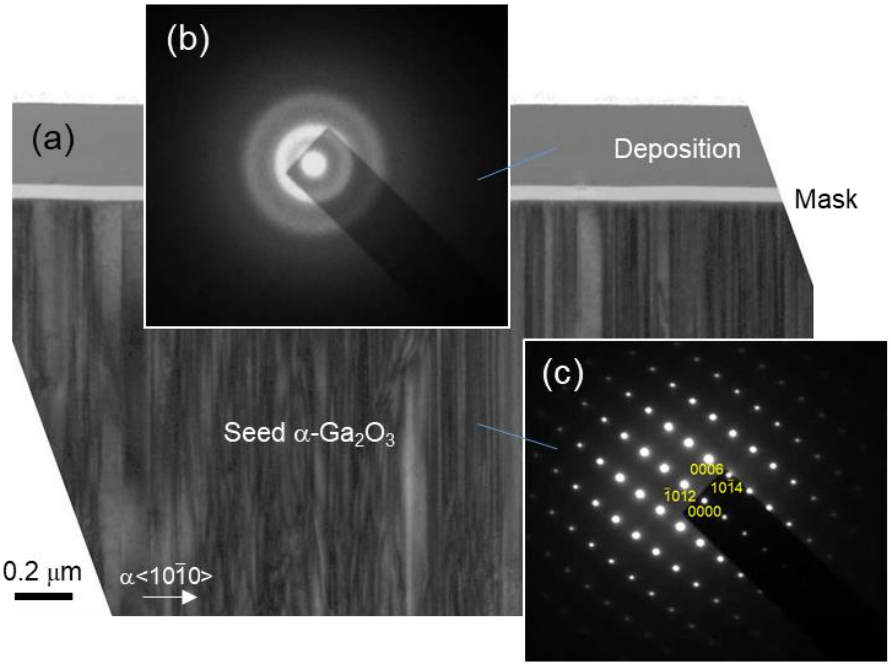

Fig. 4.

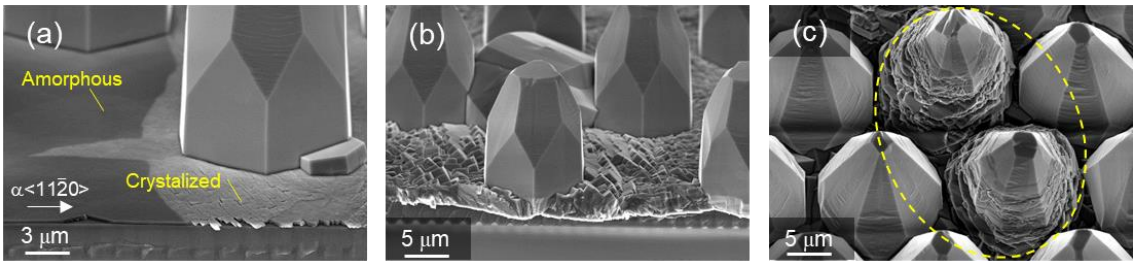

Fig. 5.

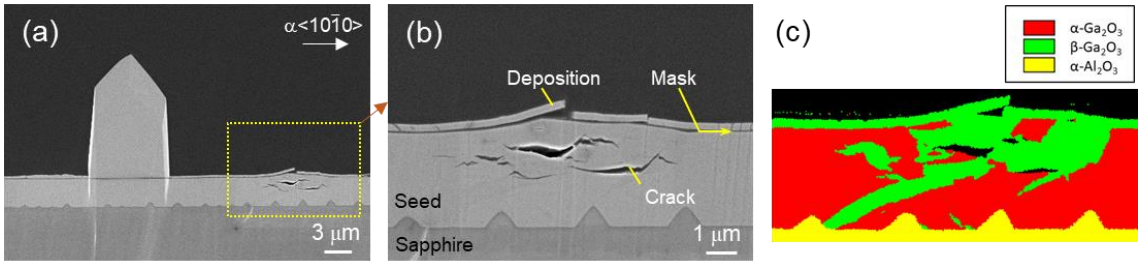
(a)
α<10$\bar{1}$0>
3 μm
(b)
Deposition
Mask
Crack
Seed
Sapphire
1 μm
(c)
α-Ga2O3
β-Ga2O3
α-Al2O3

Fig. 6.

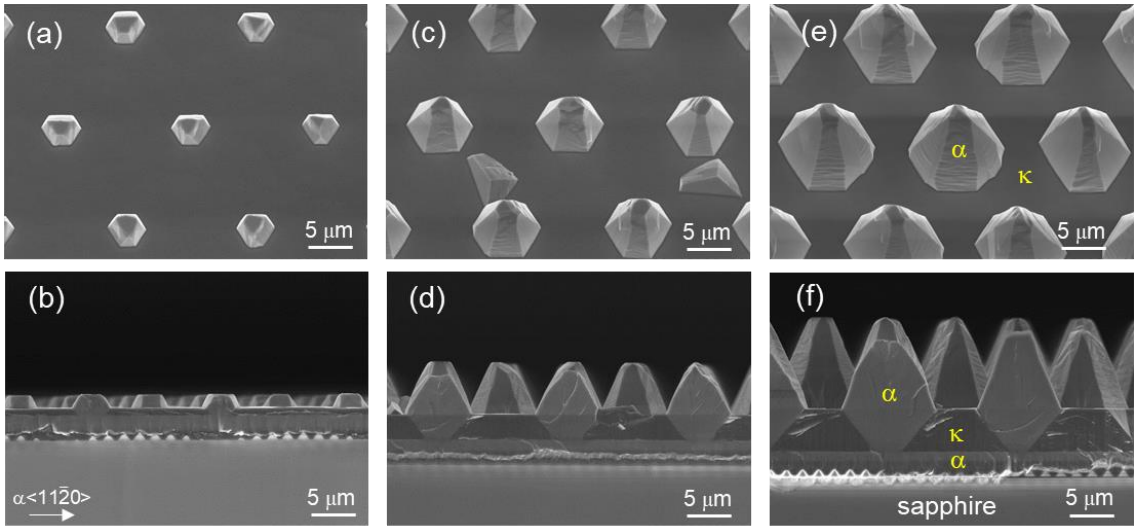
(a)
5 μm
(c)
5 μm
(e)
α
κ
5 μm
(b)
α<11$\bar{2}$0>
5 μm
(d)
5 μm
(f)
α
κ
α
sapphire
5 μm

Fig. 7.

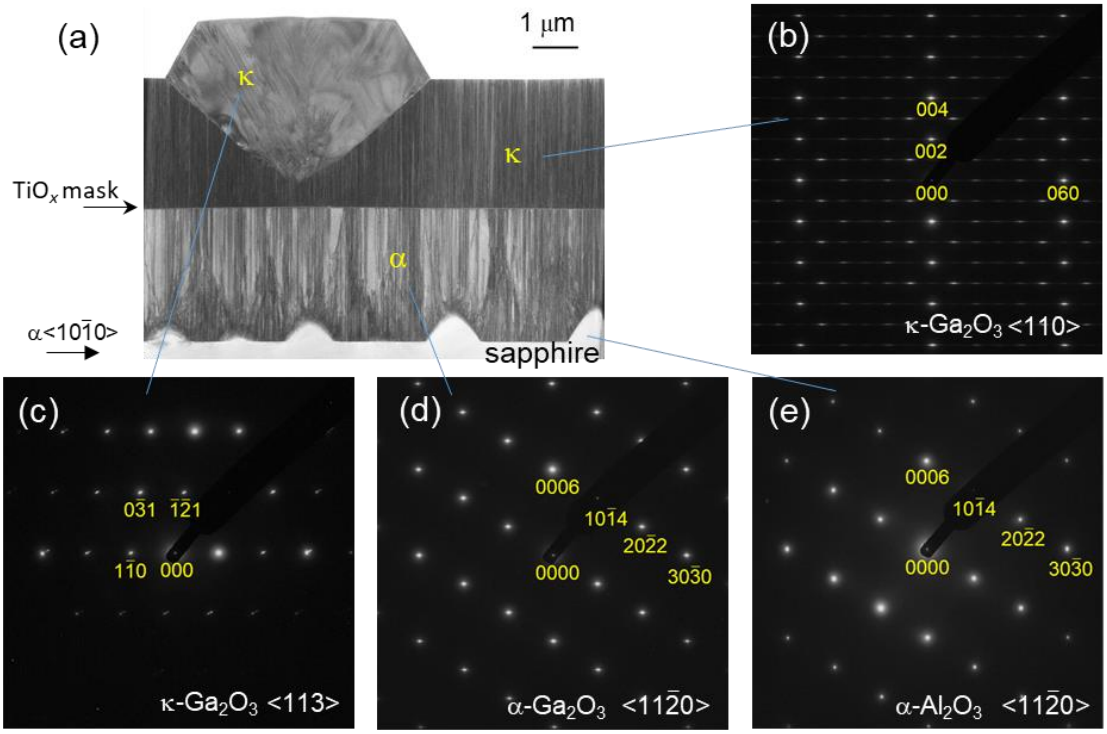
(a)
1 μm
κ
κ
α
TiO$_x$ mask
α<10$\bar{1}$0>
sapphire
(b)
004
002
000
060
κ-Ga$_2$O$_3$ <110>
(c)
03$\bar{1}$ $\bar{1}$21
1$\bar{1}$0 000
κ-Ga$_2$O$_3$ <113>
(d)
0006
10$\bar{1}$4
20$\bar{2}$2
0000
30$\bar{3}$0
α-Ga$_2$O$_3$ <11$\bar{2}$0>
(e)
0006
10$\bar{1}$4
20$\bar{2}$2
0000
30$\bar{3}$0
α-Al$_2$O$_3$ <11$\bar{2}$0>

Fig. 8.

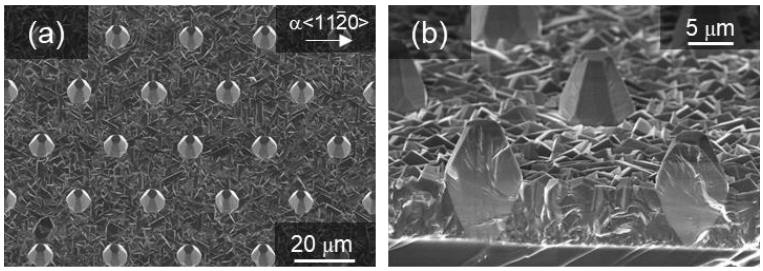
(a)
α<11$\bar{2}$0>
20 μm
(b)
5 μm

Fig. 9.

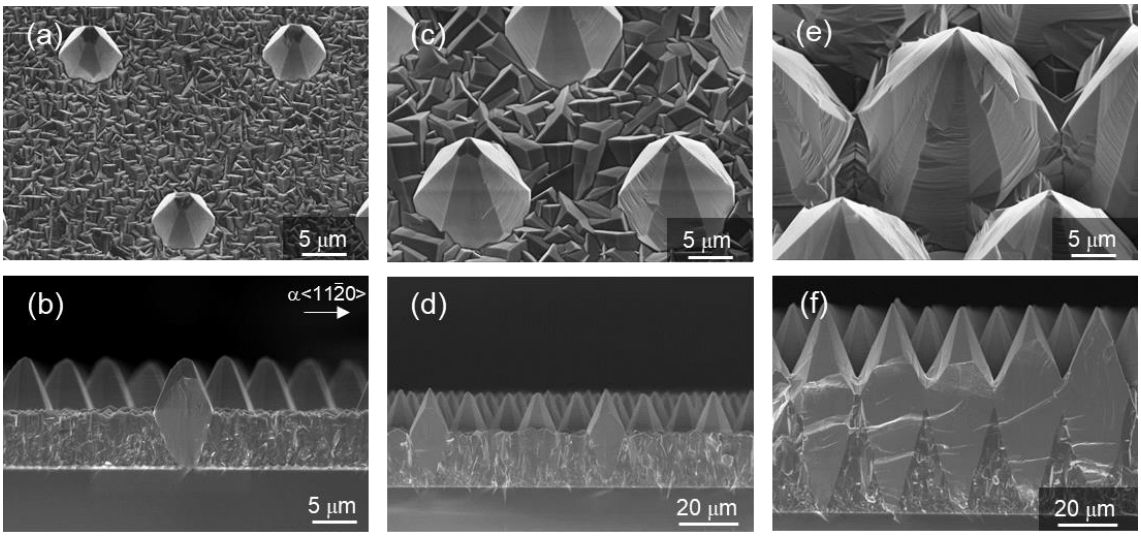
(a)
5 μm
(c)
5 μm
(e)
5 μm
(b)
α<11$\bar{2}$0>
5 μm
(d)
20 μm
(f)
20 μm

Fig. 10.

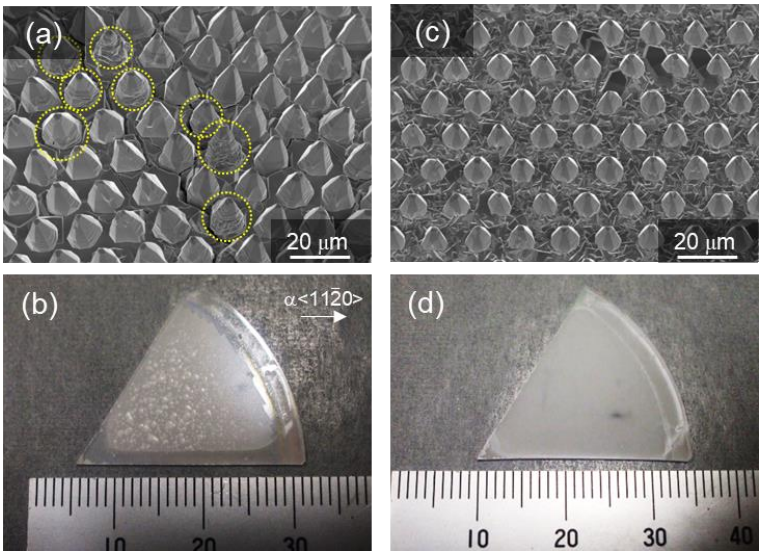
(a)
20 μm
(c)
20 μm
(b)
α<11$\bar{2}$0>
(d)
10
20
30
40

Fig. 11.

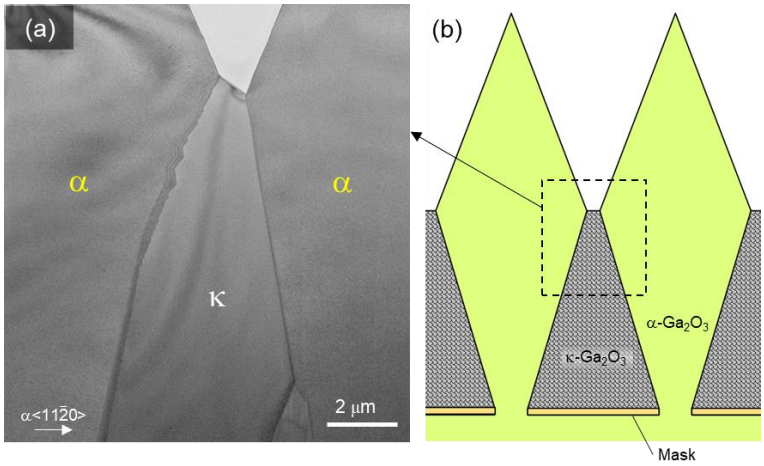
(a)
α
α
κ
α<11$\bar{2}$0>
2 μm
(b)
α-Ga2O3
κ-Ga2O3
Mask

Fig. 12.

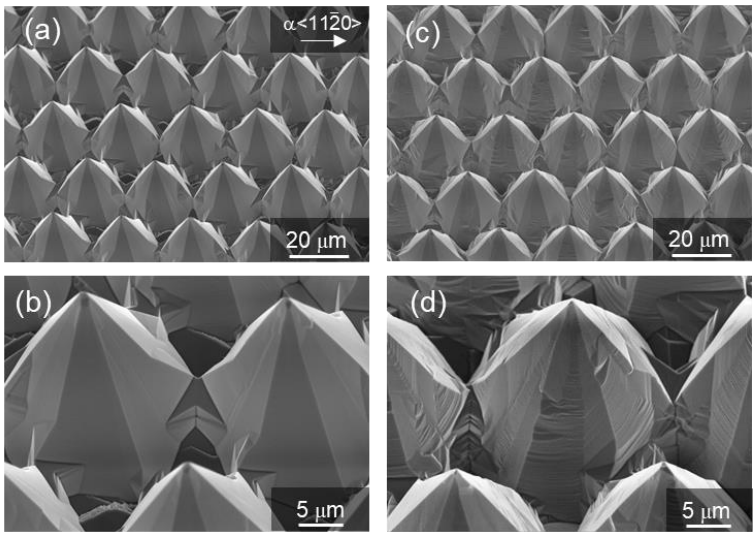

Fig. 13.